Synthesis, molecular structure, spectroscopic properties and stability of (Z)-N-methyl-C-2,4,6-trimethylphenylnitrone

ARTICLE *in* SPECTROCHIMICA ACTA PART A MOLECULAR AND BIOMOLECULAR SPECTROSCOPY · OCTOBER 2014

Impact Factor: 2.35 · DOI: 10.1016/j.saa.2014.10.096 · Source: PubMed

Spectrochimica Acta Part A: Molecular and Biomolecular Spectroscopy 136 (2015) 1857–1868

Contents lists available at ScienceDirect

Spectrochimica Acta Part A: Molecular and Biomolecular Spectroscopy

journal homepage: www.elsevier.com/locate/saa

Synthesis, molecular structure, spectroscopic properties and stability of (*Z*)-*N*-methyl-*C*-2,4,6-trimethylphenylnitrone

Jamal Lasri [a,*], Ali I. Ismail [a], Matti Haukka [c], Saied M. Soliman [a,b,*]

[a] Department of Chemistry, Rabigh College of Science and Arts, King Abdulaziz University, P.O. Box 344, Rabigh 21911, Saudi Arabia
[b] Department of Chemistry, Faculty of Science, Alexandria University, Ibrahimia, P.O. Box 426, Alexandria 21321, Egypt
[c] University of Jyväskylä, Department of Chemistry, P.O. Box 35, FI-40014 University of Jyväskylä, Finland

HIGHLIGHTS

- New *N*-methyl-*C*-2,4,6-trimethylphenylnitrone has been synthesized.
- *Z*-isomer is more stable than the *E*-one both in gas phase and in solution.
- The IR, electronic and NMR spectra were studied experimentally and theoretically.
- The studied nitrone has about five times higher NLO than urea.
- NBO analysis indicates the presence of weak C—H···O non-conventional interaction.

GRAPHICAL ABSTRACT

New *N*-methyl-*C*-2,4,6-trimethylphenylnitrone has been synthesized and characterized using FTIR, NMR, UV–Vis, high resolution mass spectrometry and X-ray diffraction. The relative stability and percentage population of its two possible isomers (*E* and *Z*) have been calculated using the B3LYP/6-311++G(d,p).

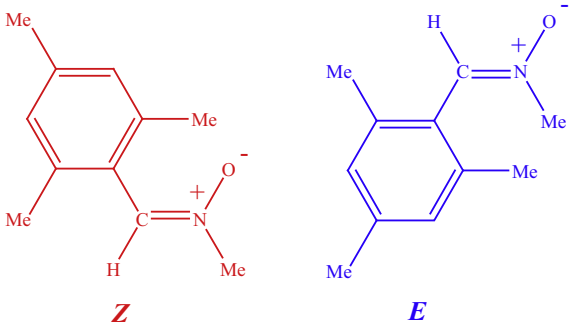

ARTICLE INFO

Article history:
Received 10 July 2014
Accepted 23 October 2014
Available online 31 October 2014

This paper is dedicated to our wonderful friend Dr. Samir Senior from Alexandria University (Egypt) who recently passed away.

Keywords:
Nitrone
B3LYP
X-ray single crystal
Electronic spectra
NBO

ABSTRACT

New *N*-methyl-*C*-2,4,6-trimethylphenylnitrone **1** has been synthesized starting from N-methylhydroxylamine and mesitaldehyde. The product was fully characterized using different spectroscopic techniques; FTIR, NMR, UV–Vis, high resolution mass spectrometry and X-ray diffraction. The relative stability and percent of population of its two possible isomers (*E* and *Z*) were calculated using the B3LYP/6-311++G(d,p) method in gas phase and in solution. In agreement with the X-ray results, it was found that *Z*-isomer is the most stable one in both gas phase and solution. The molecular geometry, vibrational frequencies, gauge-including atomic orbital (GIAO), and chemical shift values were also calculated using the same level of theory. The TD-DFT results of the studied nitrone predicted a π–π^* transition band at 285.1 nm (f_{osc} = 0.3543) in the gas phase. The rest of the spectral bands undergo either hyperchromic or hypsochromic shifts in the presence of solvent. Polarizability and HOMO–LUMO gap values were used to predict the nonlinear optical properties (NLO) of the studied compound. NBO analysis has been used to determine the most accurate Lewis structure of the studied molecule.

Introduction

Nitrones, whose name comes from nitrogen ketone, have been widely reviewed and illustrated in synthetic chemistry [1,2].

* Corresponding authors at: Department of Chemistry, Rabigh College of Science and Arts, King Abdulaziz University, P.O. Box 344, Rabigh 21911, Saudi Arabia. Tel.: +966 560247664 (J. Lasri). Tel:. +966 565450752 (S.M. Soliman).
E-mail addresses: jlasri@kau.edu.sa (J. Lasri), saied1soliman@yahoo.com (S.M. Soliman).

http://dx.doi.org/10.1016/j.saa.2014.10.096
1386-1425/

Nitrone derivatives have been used for the synthesis of many natural products of biological interesting materials [3]. These compounds were found to act as an important key step in the efficient incorporation of multiple stereocenters *via* cycloaddition reactions [4]. The nitrone moiety has possessed pharmacological activity that provides the effective center in the molecular structure of many drugs [5]. This makes nitrones a potential candidates in many experimental animal models as biological active materials [6,7] and as anti-cancer drugs [8]. A combination of nitrones and anti-oxidants was found to have a synergistic effect to prevent the acute acoustic noise-induced hearing loss [9]. The corrosion of metals and alloys in organic acidic media was significantly lowered when treated by nitrones [10–13].

Inouye et al. [14] proposed that crystalline nitrones exist as mainly *Z*-isomer. They also found that the *E*/*Z* isomerization occurred when it dissolved. There are only few publications that deal with the theoretical studies on the molecular structure and spectral properties of nitrones [15,16].

In this work, the new *N*-methyl-*C*-2,4,6-trimethylphenylnitrone **1** is synthesized and characterized using FTIR, ^{1}H, ^{13}C NMR, mass spectrometry and X-ray diffraction. We have studied the equilibrium between the *E* and *Z* isomers in gas phase and in various solvents (with different polarity) to predict the effect of solvent on the vibrational, electronic, and NMR spectra of the most stable isomer. Frontier molecular orbitals (FMOs) and natural atomic charges were calculated at the same level of theory. Natural bond orbital (NBO) calculations were performed to predict the most accurate Lewis structure of the studied nitrone. Also, the stabilization energy of various intramolecular interactions was investigated.

Experimental section

Material and instrumentation

All solvents and reagents were obtained from Sigma–Aldrich and were used as received. ^{1}H and ^{13}C NMR spectra (in $CDCl_3$) were measured on Bruker Avance III HD 600 MHz (Ascend™ Magnet) spectrometer at ambient temperature. ^{1}H and ^{13}C chemical shifts (δ) are expressed in ppm relative to $Si(Me)_4$. Infrared spectra (400–4000 cm^{-1}) were recorded on an Alpha Bruker FT-IR instrument in KBr pellets. Mass spectra were carried out using high resolution ion-trap time-of-flight mass spectrometry interfaced with electrospray source (MicrOTOF II mass spectrometry from Bruker). The drying gas temperature of the mass spectrometry was maintained at 200 °C. N_2 was used as nebulizer gas at a pressure of 20 psi. Positive mode scanning was performed at the range of *m*/*z* 50–1500. Acetonitrile solution of the product compound (nitrone) was continuously introduced into the mass spectrometer detector with a syringe pump at a flow rate of 20 μL/min. The electrospray voltage and the collision cell RF were set at 2.5 kV and 100 Vpp, respectively. Tandem mass spectrometry was applied to the trapped peak at *m*/*z* 178.1233 with collision energy (CID) set at 35 eV. The accuracy of the mass spectrometer was enough to assign the fragmentation species as good as 5 ppm as shown in Fig. S1 (Supplementary Information). Liquid chromatography (Agilinet series 1260) was used to separate and measure the UV/Vis spectrum for the nitrone compound in aqueous medium. Five microliter of acetonitrile solution (1 mg of nitrone/mL) was introduced into HPLC instrument that is coupled with UV/Vis detector. Acetonitrile/water mixture (30:70) was used as mobile phase at a flow rate of 1.0 mL/min for 2 min. After that, the mixture was set at 100% water for another 10 min. Full scan UV/Vis spectrum was measured for the separated nitrone peak at retention time = 3.8 min, which means that the spectrum was recorded in 100% water.

Synthesis of (Z)-N-methyl-C-2,4,6-trimethylphenylnitrone ***1***

Sodium carbonate (0.63 g, 5.98 mmol) was added to a solution of N-methylhydroxylamine hydrochloride (1.00 g, 11.97 mmol) in

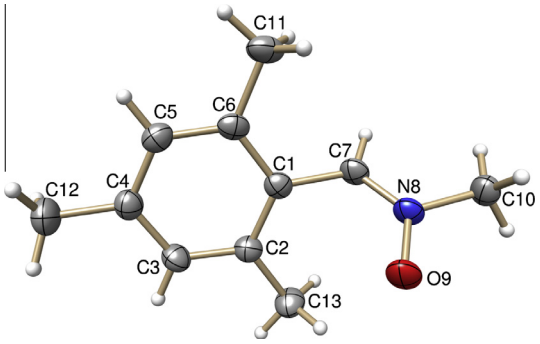

Fig. 1. Thermal ellipsoid plot of **1**. The thermal ellipsoids are drawn at 50% probability.

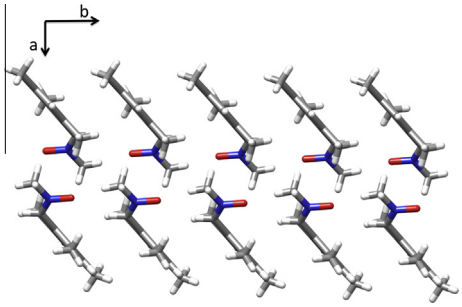

Fig. 2. Packing of **1** viewed along crystallographic *c*-axis.

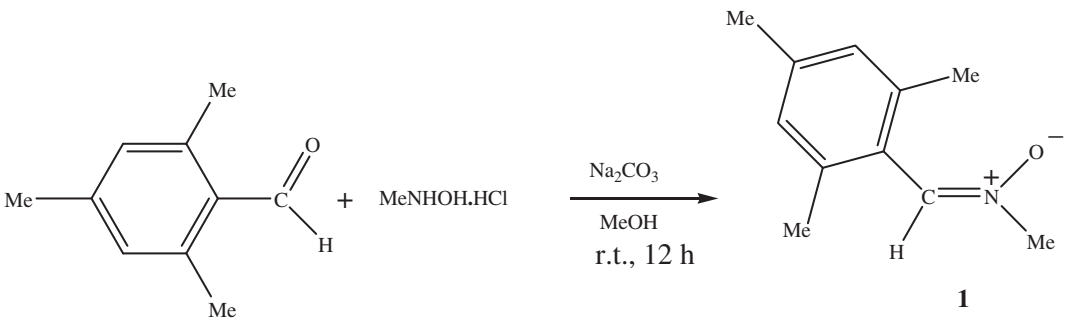

Scheme 1. Synthesis of acyclic nitrone **1**.

methanol (4 mL). The mixture was stirred for 5 min. Mesitaldehyde (1.61 g, 10.88 mmol) was then added and the mixture was stirred at room temperature for 12 h. The precipitate formed during the reaction was filtered off and the filtrate was evaporated to dryness to provide further solid. The precipitate was then dissolved in dichloromethane resulting in the precipitation of NaCl. The latter was filtered off and the dichloromethane was then removed *in vacuo*. The final yellow-white solid was washed with ether to obtain pure (*Z*)-*N*-methyl-*C*-2,4,6-trimethylphenylnitrone **1** in *c.a.* 90% yield (Scheme 1).

$^{-}O^{+}N(Me)$═C(H)($C_6H_2Me_3$-2,4,6)

Yield: 90%. IR (cm^{-1}): 1610 (C═N). ^{1}H NMR ($CDCl_3$), δ: 2.28 and 2.30 (two s, 6H and 3H, respectively, CH_3Ph), 3.94 (s, 3H, CH_3N), 6.90 (s, 2H, C$H_{aromatic}$), 7.61 (s, 1H, C(*H*)═N). ^{13}C NMR ($CDCl_3$), δ: 19.8 and 21.1 (*C*H_3Ph), 53.2 (*C*H_3N), 125.7 ($C_{aromatic}$), 128.4 (*C*$H_{aromatic}$), 135.7 (*C*(H)═N), 137.5 and 139.5 ($C_{aromatic}$). DEPT-135 NMR ($CDCl_3$), δ: 19.8 and 21.1 (*C*H_3Ph), 53.2 (*C*H_3N), 128.4 (*C*$H_{aromatic}$) and 135.7 (*C*(H)═N). ESI$^+$-MS, *m*/*z*: 178.1233 [M+H]$^+$. Tandem MS (for 178.12), *m*/*z*: 178.1233, 160.1127, 146.0955, 131.0733, 119.0849, 105.0065, 91.0483. 73.068. UV/Vis, wavelength maxima: 210, 224, 250 and 278 nm.

X-ray crystallography

The X-ray diffraction data of **1** (Figs. 1 and 2) was collected on an Agilent Technologies Supernova diffractometer using Cu Kα radiation (λ = 1.5418 Å). The *CrysAlisPro* [17] program package was used for cell refinements and data reductions. A multi-scan absorption correction based on equivalent reflections (*CrysAlisPro*) [17] was applied to the data. The structure was solved by direct method using the *SHELXL-97* [18] program with the *Olex2* [19] graphical user interface. Structural refinement was carried out using *SHELXL-97* [18]. Molecular graphics was created with the *UCSF Chimera* package [20]. Hydrogen atoms were positioned geometrically and constrained to ride on their parent atoms with C—H = 0.93–0.96 Å and U_{iso} = 1.2–1.5 U_{eq} (parent atom). The crystallographic details are summarized in Table 1. Selected bond lengths and angles for **1** were tabulated in Table 2. For additional information regarding other X-ray data see Supplementary Information (Tables S1–S5).

Table 1
Crystal data for the studied nitrone **1**.

	1
Empirical formula	$C_{12}H_{15}NO$
Fw	176.99
Temp. (K)	293(2)
λ (Å)	1.5418
Crystsyst	Monoclinic
Space group	*C*2/*c*
a (Å)	25.6557(11)
b (Å)	5.0634(2)
c (Å)	15.7014(6)
β (deg)	102.554(4)
V (Å^3)	1990.92(14)
Z	8
ρ_{calc} (Mg/m^3)	1.181
μ(Mo Kα) (mm^{-1})	0.568
No. reflns.	9680
Unique reflns.	2073
GOOF (F^2)	1.046
R_{int}	0.1273
$R1^a$ ($I \geqslant 2\sigma$)	0.0737
$wR2^b$ ($I \geqslant 2\sigma$)	0.2028

[a] $R1 = \Sigma||F_o| - |F_c||/\Sigma|F_o|$.
[b] $wR2 = [\Sigma[w(F_o^2 - F_c^2)^2]/\Sigma[w(F_o^2)^2]]^{1/2}$.

Computational details

A complete optimization was done on the two isomeric forms *Z* and *E* by minimizing the energies with respect to all geometrical parameters without imposing any molecular symmetry constraints. The DFT-B3LYP/6-311++G(d,p) method was used for the complete optimization using Gaussian 03 program [21]. The structures of the optimized geometries were drawn by GaussView 4.1 [22]. The computational study was first carried out in gas phase. After that the self-consistent reaction field (SCRF) theory [23], with polarized continuum model (PCM), was used to predict the effect of solvent on the stability of the studied isomers [24]. The stability of the optimized geometry was confirmed by frequency calculations, which gave no imaginary values for the frequencies. The total energy distribution (TED) of the vibrational modes of the molecules was calculated with the VEDA program [25]. They were characterized by their total energy distribution (TED%). UV absorption energies of this compound were calculated by the TD-DFT method in different solvents to predict the effect of solvent on the electronic spectra compared to the gas phase, also for visualizing HOMO and LUMO states. The natural atomic charges are calculated using NBO calculations as implemented in the Gaussian 03 package [26] at the DFT/B3LYP level. The most accurate Lewis structure and the different intermolecular charge transfer interaction (ICT) energies were investigated using the NBO calculations. The gauge including atomic orbital (GIAO) method was used for the NMR calculations. The ^{1}H and ^{13}C isotropic tensors referenced to the TMS calculations were carried out at the same level of theory.

Table 2
Selected bond lengths (Å) and angles (°) for the studied nitrone **1**.

O9—N8	1.290(2)
N8—C7	1.301(2)
N8—C10	1.471(2)
C7—C1	1.474(2)
O9—N8—C7	125.00(14)
O9—N8—C10	114.82(14)
C7—N8—C10	120.13(14)
N8—C7—C1	124.08(15)

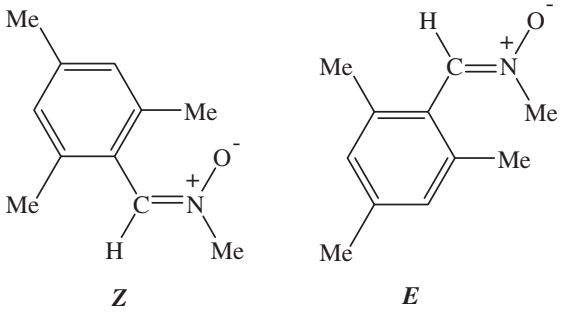

Scheme 2. The *Z* and *E* isomers of the studied nitrone **1**.

Table 3
Effect of solvent on the population percentages (%) of the studied isomers.

Isomer	Pop. (%)				
	Gas	Cyclohexane	Chloroform	DMSO	Water
Z	99.18	98.06	95.28	91.14	93.88
E	0.82	1.94	4.72	8.86	6.12

Table 4
Comparative experimental and angles of the *Z*-isomer in gas phase and in solvents of different polarities.

Parameter[a]	Gas (ε = 0)	Cyclohexane (ε = 2.02)	Chloroform (ε = 4.90)	DMSO (ε = 46.70)	Water (ε = 78.39)	X-ray
R(1-2)	1.281	1.285	1.290	1.296	1.297	1.290
R(2-3)	1.317	1.314	1.313	1.310	1.309	1.301
R(2-16)	1.482	1.481	1.480	1.479	1.479	1.471
R(3-4)	1.084	1.085	1.086	1.088	1.088	0.930
R(3-5)	1.466	1.468	1.469	1.471	1.471	1.474
R(5-10)	1.416	1.416	1.416	1.415	1.416	1.406
R(5-11)	1.420	1.419	1.419	1.417	1.418	1.415
R(6-7)	1.088	1.089	1.089	1.090	1.090	0.931
R(6-11)	1.395	1.396	1.397	1.398	1.398	1.393
R(6-20)	1.401	1.402	1.402	1.402	1.402	1.390
R(8-9)	1.088	1.088	1.089	1.090	1.090	0.930
R(8-10)	1.401	1.401	1.402	1.401	1.402	1.394
R(8-20)	1.396	1.397	1.398	1.399	1.399	1.390
R(10-12)	1.507	1.507	1.508	1.509	1.509	1.504
R(11-21)	1.513	1.513	1.513	1.513	1.513	1.506
R(12-13)	1.097	1.097	1.097	1.097	1.097	0.960
R(12-14)	1.093	1.093	1.093	1.093	1.093	0.961
R(12-15)	1.096	1.096	1.096	1.096	1.096	0.960
R(16-17)	1.091	1.091	1.092	1.092	1.092	0.961
R(16-18)	1.091	1.091	1.091	1.091	1.090	0.960
R(16-19)	1.092	1.092	1.092	1.092	1.092	0.961
R(20-25)	1.511	1.511	1.511	1.511	1.511	1.510
R(21-22)	1.096	1.096	1.096	1.096	1.096	0.959
R(21-23)	1.093	1.093	1.093	1.093	1.093	0.960
R(21-24)	1.098	1.098	1.098	1.097	1.097	0.959
R(25-26)	1.095	1.095	1.095	1.095	1.095	0.959
R(25-27)	1.094	1.094	1.094	1.094	1.094	0.960
R(25-28)	1.097	1.098	1.098	1.098	1.098	0.961
R(1---15)	2.207	2.228	2.258	2.290	2.289	2.305
A(1-2-3)	125.987	125.737	125.507	125.209	125.231	124.994
A(1-2-16)	114.140	114.246	114.369	114.405	114.434	114.819
A(3-2-16)	119.873	120.016	120.123	120.386	120.334	120.139
A(2-3-4)	114.648	114.753	114.864	115.145	115.064	117.933
A(2-3-5)	125.611	125.478	125.281	124.796	124.939	124.087
A(2-16-17)	107.316	107.414	107.520	107.650	107.654	109.453
A(2-16-18)	111.223	111.081	110.903	110.723	110.673	109.447
A(2-16-19)	107.497	107.558	107.611	107.661	107.675	109.433
A(4-3-5)	119.609	119.670	119.782	120.018	119.945	117.980
A(3-5-10)	122.554	122.358	122.207	121.786	121.890	122.886
A(3-5-11)	117.646	117.751	117.842	118.106	118.003	117.084
A(10-5-11)	119.725	119.811	119.866	120.021	120.014	119.975
A(5-10-8)	118.666	118.695	118.733	118.748	118.741	118.897
A(5-10-12)	121.968	121.857	121.788	121.588	121.630	121.924
A(5-11-6)	119.351	119.292	119.248	119.157	119.160	118.836
A(5-11-21)	121.137	121.103	121.097	121.071	121.072	121.259
A(7-6-11)	118.896	118.895	118.893	118.890	118.895	119.138
A(7-6-20)	119.297	119.316	119.332	119.369	119.368	119.057
A(11-6-20)	121.803	121.786	121.772	121.739	121.736	121.805
A(6-11-21)	119.496	119.589	119.639	119.757	119.755	119.893
A(6-20-8)	117.995	118.053	118.109	118.194	118.203	118.506
A(6-20-25)	120.773	120.763	120.739	120.790	120.771	120.980
A(9-8-10)	118.404	118.478	118.537	118.629	118.618	119.016
A(9-8-20)	119.174	119.194	119.224	119.257	119.265	119.074
A(10-8-20)	122.418	122.325	122.235	122.109	122.113	121.910
A(8-10-12)	119.333	119.417	119.444	119.637	119.596	119.145
A(8-20-25)	121.214	121.167	121.135	120.997	121.006	120.509
A(10-12-13)	111.121	111.174	111.205	111.220	111.202	109.442
A(10-12-14)	110.822	110.835	110.825	110.817	110.799	109.515
A(10-12-15)	110.650	110.620	110.669	110.654	110.705	109.462
A(11-21-22)	111.712	111.684	111.699	111.695	111.713	109.430
A(11-21-23)	110.687	110.695	110.682	110.699	110.681	109.489
A(11-21-24)	111.933	111.877	111.806	111.722	111.687	109.535
A(13-12-14)	107.925	107.942	107.976	107.938	107.959	109.416
A(13-12-15)	106.780	106.830	106.811	107.064	107.020	109.488
A(14-12-15)	109.416	109.314	109.225	109.023	109.028	109.504
A(17-16-18)	110.995	110.934	110.892	110.824	110.828	109.550
A(17-16-19)	109.071	109.151	109.259	109.360	109.375	109.549
A(18-16-19)	110.608	110.581	110.545	110.522	110.536	109.396
A(20-25-26)	111.365	111.348	111.337	111.365	111.360	109.506
A(20-25-27)	111.388	111.382	111.380	111.374	111.374	109.471
A(20-25-28)	111.115	111.079	111.031	110.956	110.942	109.495
A(22-21-23)	107.922	107.942	107.968	107.979	108.004	109.464
A(22-21-24)	107.107	107.083	107.033	106.957	106.944	109.429
A(23-21-24)	107.257	107.343	107.442	107.582	107.608	109.481

Table 4 (*continued*)

Parameter[a]	Gas ($\varepsilon = 0$)	Cyclohexane ($\varepsilon = 2.02$)	Chloroform ($\varepsilon = 4.90$)	DMSO ($\varepsilon = 46.70$)	Water ($\varepsilon = 78.39$)	X-ray
A(26-25-27)	108.057	108.122	108.213	108.343	108.361	109.499
A(26-25-28)	107.204	107.186	107.153	107.176	107.166	109.479
A(27-25-28)	107.516	107.531	107.538	107.438	107.449	109.378

[a] Atom numbering are referred to Fig. 3.

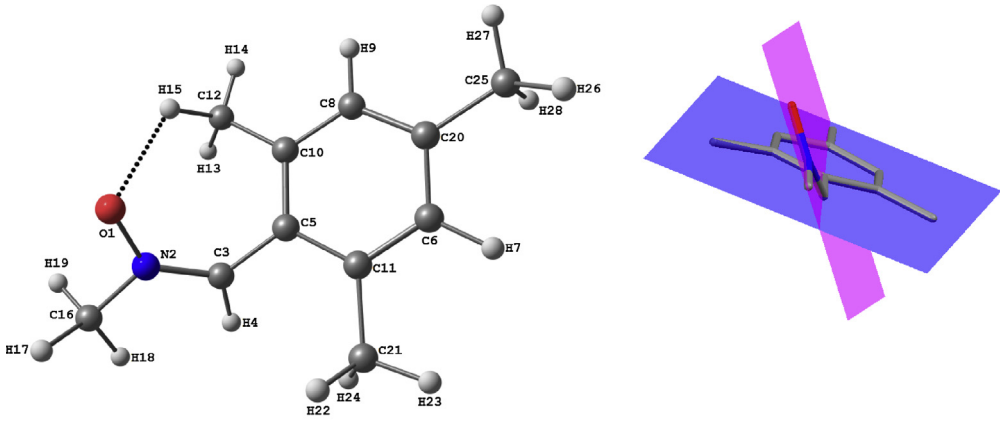

***Z*-isomer**

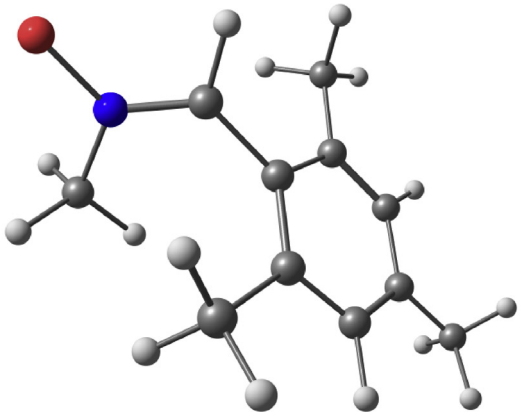

***E*-isomer**

Fig. 3. The optimized molecular structure of the *E*- and *Z*-isomers calculated using the B3LYP/6-311++G(d,p) method.

Results and discussion

Stability and thermodynamic results

The studied nitrone **1** is capable of existing in two isomeric structures; either the *E* or *Z* configuration. The possible isomers of the studied compound are given in Scheme 2. The B3LYP/6-311++G(d,p) calculated energy predictions of the studied isomers are compared in Table S6 (Supplementary Information). The results showed that the *Z*-isomer has the lowest energy value ($E = 557.9293$ Hartrees) in the gas phase. The *E*-isomer is higher in energy by only 2.86 kcal/mol. This suggests that nitrone isomers capable of *E*/*Z* isomerization even at room temperature. The relative abundances of the *Z*- and *E*-isomers were calculated using Gibbs free energy equation; $\Delta G = -RT\ln K$. (where ΔG denotes the difference between the Gibbs free energies of *E*-isomer relative to the *Z*-one and *K* is the corresponding equilibrium constant). The abundance of the most stable species, *Z* is equal to 99.18% at 298 K in gas phase. This indicates that the *Z*-isomer is the predominant in the gas phase. These results are in good agreement with the experimentally measured X-ray structure.

Solvent effects are important on the stability of isomers, since polarity differences among isomers can make significant changes in their relative energies in solution. We used PCM calculations to analyze the effect of solvent on the stability of the studied isomers. Table S6 (Supplementary Information) shows the total energies and thermodynamic parameters of the studied isomers in the presence of solvents of different polarities. The effect of different solvents on the calculated population percentage of the *E* and *Z* isomers is shown in Table 3. In solution, the energy barrier (ΔE) between the *Z*-isomer and the *E*-one decreased compared to the gas phase. As expected, it is revealed that the population as well as the stability of the more polar isomer (*E*) increases in presence of solvent compared to the gas phase. Also, the stability and the

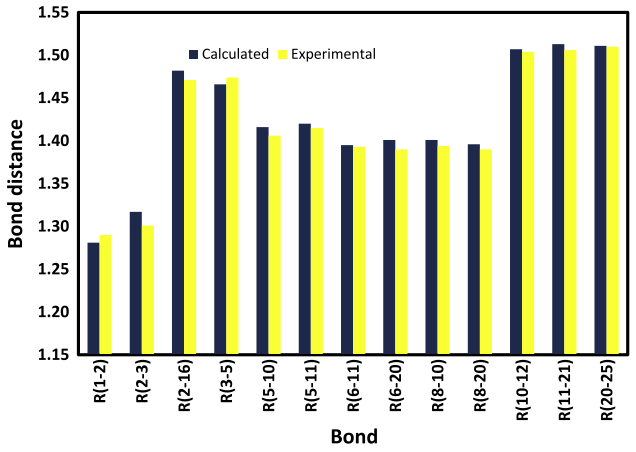

Fig. 4. Comparison between the calculated and experimental bond distances of the *Z*-isomer.

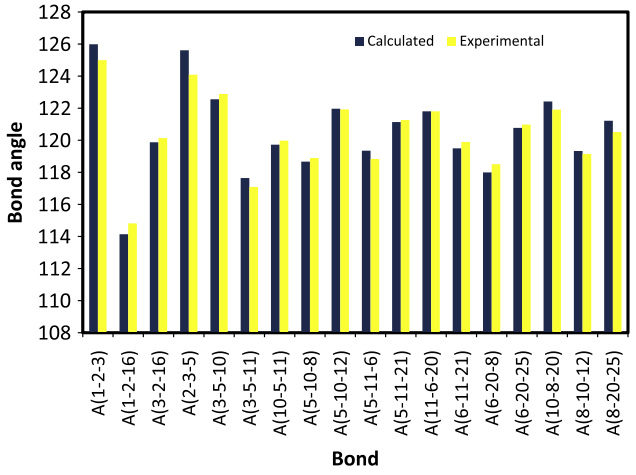

Fig. 5. Comparison between the calculated and experimental bond angles of the *Z*-isomer.

percentage population of the *E*-isomer are higher in polar solvents such as DMSO and water compared to the nonpolar medium (cyclohexane).

Molecular geometry

The optimized bond lengths and bond angles obtained for the stable *Z*-isomer using the B3LYP method with 6-311++G(d,p) basis set are given in Table 4 (the atom numbering of the optimized structure are given in Fig. 3). The optimized geometry is compared with the structural parameters obtained from the CIF file. The point group of the most stable isomer (*Z*) is C_1. Comparison between the experimental and the calculated geometric parameters (bond distances and bond angles) is shown in Figs. 4 and 5. All bond lengths are found to be overestimated except for the O1—N2 and C3—C5. The maximum deviation of the predicted values from the experimental data is 0.016 Å. These deviations are attributed to the phase difference between the calculations and the experiment. The calculations refer to an isolated molecule in the gas phase, whereas the experimental data are those of the molecule in the solid phase. The maximum deviation of the calculated bond angles from the experimental data is 1.524° (N2—C3—C5). The calculated angle between the phenyl ring plane and the plane passing through the C5—C3—N2—C16 is 51.82° (Fig. 3). The results indicate that the nitrone moiety is not coplanar with the benzene ring which agrees with the X-ray structure analysis. The H15---O1 intramolecular distance is predicted to be 2.207 Å which might indicate the presence of weak C—H---O interaction between the O-atom of the nitrone and the H-atom of the neighboring methyl group.

Table 5
The calculated natural charges of the *Z*-isomer in the gas phase and in solution using B3LYP/6-311++G(d,p) method.

Atom	Gas	Cyclohexane	Chloroform	DMSO	Water
O1	−0.5445	−0.5707	−0.5974	−0.6267	−0.6314
N2	0.0703	0.0680	0.0652	0.0610	0.0601
C3	−0.0054	0.0056	0.0167	0.0304	0.0322
H4	0.2234	0.2307	0.2400	0.2519	0.2548
C5	−0.1281	−0.1310	−0.1345	−0.1371	−0.1389
C6	−0.2508	−0.2538	−0.2570	−0.2602	−0.2606
H7	0.2299	0.2353	0.2412	0.2475	0.2488
C8	−0.2357	−0.2403	−0.2452	−0.2501	−0.2506
H9	0.2317	0.2363	0.2415	0.2471	0.2483
C10	0.0257	0.0224	0.0189	0.0146	0.0135
C11	0.0294	0.0301	0.0303	0.0294	0.0296
C12	−0.6816	−0.6824	−0.6829	−0.6845	−0.6845
H13	0.2306	0.2321	0.2342	0.2380	0.2385
H14	0.2293	0.2313	0.2336	0.2365	0.2369
H15	0.2711	0.2671	0.2627	0.2569	0.2563
C16	−0.4622	−0.4630	−0.4637	−0.4642	−0.4640
H17	0.2459	0.2476	0.2485	0.2488	0.2487
H18	0.2204	0.2258	0.2316	0.2379	0.2387
H19	0.2446	0.2465	0.2478	0.2489	0.2489
C20	−0.0162	−0.0156	−0.0155	−0.0164	−0.0162
C21	−0.6772	−0.6795	−0.6821	−0.6843	−0.6847
H22	0.2398	0.2414	0.2423	0.2426	0.2429
H23	0.2380	0.2397	0.2416	0.2432	0.2434
H24	0.2306	0.2334	0.2370	0.2412	0.2417
C25	−0.6706	−0.6727	−0.6747	−0.6765	−0.6767
H26	0.2369	0.2385	0.2400	0.2408	0.2410
H27	0.2356	0.2369	0.2381	0.2395	0.2397
H28	0.2390	0.2404	0.2419	0.2436	0.2438

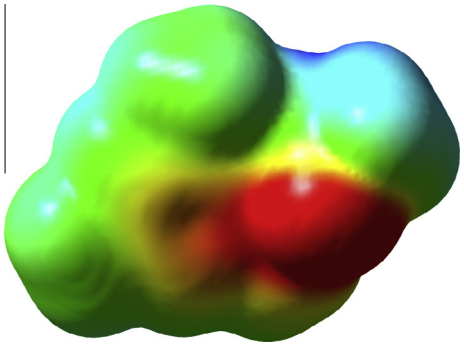

Fig. 6. Molecular electrostatic potentials (MEP) mapped on the electron density surface calculated by the DFT/B3LYP method for the most stable isomer (*Z*).

The solvent effect on the computed bond distances in solution is almost insignificant in the nonpolar solvent such as cyclohexane. In contrast, there is a noticeable change in the C—N and N—O bond distances in polar solvents. These bonds are of high polarity and can be involved in the solute–solvent interactions when using polar solvents. [27]. In general, the C—N bonds are shortened whereas the N—O bond distances are elongated due to solvent effect in solution. The changes are found to increase with the increase in the solvent polarity. Moreover, the C—H---O interaction are of little importance in solution especially in solvents of high polarity.

Natural atomic charges

The natural atomic charges (NAC) at different atomic sites of the most stable isomer (*Z*), calculated using the DFT/B3LYP

Table 6
The calculated electronic spectra using the TD-DFT method.

Solvent	λ_{max}	f_{osc}	Major contribution	Solvent	λ_{max}	f_{osc}	Major contribution
Gas	285.1	0.3543	HOMO → LUMO (74%)	Cyclohexane	288.4	0.4254	HOMO → LUMO (78%)
	244.1	0.0494	H − 1 → LUMO (11%) + HOMO → L + 2 (71%)		242.7	0.0644	HOMO → L + 2 (73%)
	217.2	0.0171	H − 2 → L + 1 (92%)		211.7	0.0610	H − 2 → L + 1 (14%) + H − 1 → L + 2 (10%) + HOMO → L + 6 (67%)
	205.9	0.1273	H − 2 → L + 2 (27%) + H − 1 → L + 2 (25%) + HOMO → L + 8 (24%)		204.8	0.1220	H − 3 → L + 1 (12%) + H − 2 → L + 2 (52%) + H − 1 → L + 2 (16%)
Chloroform	287.2	0.4132	HOMO → LUMO (78%)	DMSO	284.4	0.3492	HOMO → LUMO (73%)
	240.8	0.0624	HOMO → L + 2 (70%)		238.4	0.0491	H − 1 → L + 3 (14%) + HOMO → L + 1 (62%)
	208.0	0.0900	H − 1 → L + 2 (19%) + HOMO → L + 6 (64%)		201.3	0.0532	H − 3 → L + 1 (10%) + H − 2 → L + 2 (39%) + HOMO → L + 6 (20%)
	205.2	0.0739	H − 2 → L + 1 (10%) + H − 1 → L + 2 (19%) + HOMO → L + 6 (23%) + HOMO → L + 7 (12%)		195.4	0.3532	H − 2 → L + 1 (24%) + H − 1 → L + 3 (20%)
Water	283.5	0.3395	HOMO → LUMO (74%)				
	238.1	0.0465	H − 1 → L + 3 (14%) + HOMO → L + 1 (65%)				
	200.6	0.0536	H − 2 → L + 2 (44%) + HOMO → L + 6 (13%)				
	194.6	0.3329	H − 2 → L + 1 (25%) + H − 1 → L + 3 (21%)				

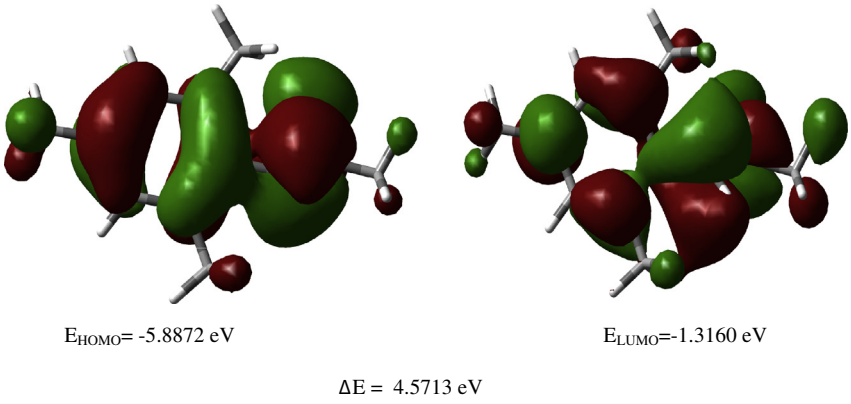

Fig. 7. The ground state isodensity surface plots for the frontier molecular orbitals (MOs) contributed in the electronic transitions of the most stable isomer (*Z*).

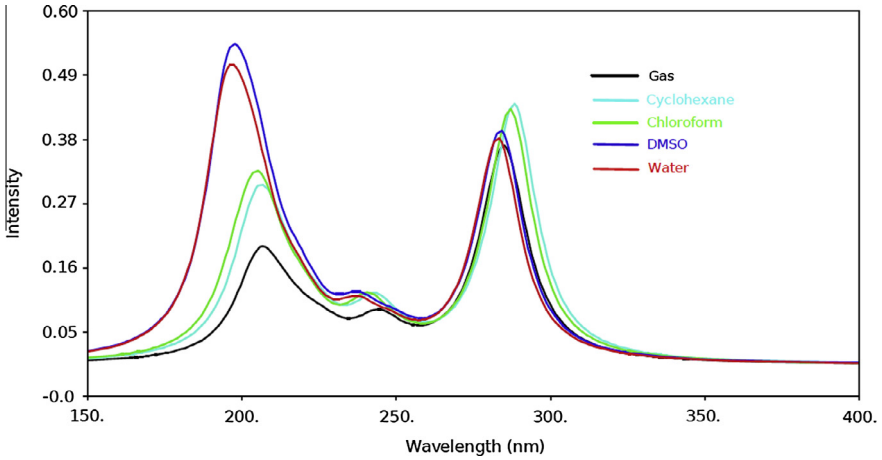

Fig. 8. The calculated electronic spectra of the *Z*-isomer in gas phase and in different solvents using TD-DFT method.

method, are collected in Table 5. From the NAC values listed in this table, we can observe the electropositive nature of hydrogen atoms. All the hydrogen atoms have positive charges within range from 0.2234 to 0.2711 in the gas phase. Of these H-sites, the H17 has the highest positive charge density probably due to the C—H---O interaction. The highest negative charge densities occur at the oxygen atom. Since the O-atom is more electronegative than nitrogen so the latter has positive charge. The largest variation of the NAC values due to the solvent occurs at the O1 atom. The presence of solvent increases the negative charge density at O-atom. The change in the charge density at the O-site is higher in polar solvents than in the nonpolar solvent. The O-atom locates at terminal position in the molecule which makes them affected most by the solvent.

Table 7
The calculated chemical shifts δ (ppm) of *Z*-nitrone using GIAO method.

Atom	δ_{calc} (ppm)					$\delta_{exp.}$ (ppm)
	Gas	Cyclohexane	Chloroform	DMSO	Water	
H4	7.98	8.14	8.33	8.60	8.66	7.61
H7	7.26	7.39	7.53	7.70	7.73	6.90
H9	7.29	7.37	7.49	7.60	7.63	6.90
H13	2.04	2.12	2.19	2.37	2.37	2.28
H14	2.26	2.27	2.31	2.33	2.35	2.28
H15	3.90	3.79	3.64	3.46	3.45	2.28
H17	4.07	4.10	4.11	4.10	4.10	3.94
H18	3.84	3.92	4.01	4.11	4.13	3.94
H19	4.02	4.06	4.09	4.09	4.10	3.94
H22	2.64	2.65	2.65	2.62	2.62	2.28
H23	2.24	2.28	2.34	2.39	2.39	2.28
H24	2.62	2.65	2.71	2.78	2.79	2.28
H26	2.54	2.57	2.60	2.56	2.57	2.30
H27	2.31	2.33	2.36	2.41	2.42	2.30
H28	2.85	2.87	2.89	2.88	2.88	2.30
C3	122.69	124.66	126.89	129.63	130.02	135.7
C5	115.92	116.00	116.09	116.26	116.14	137.5
C6	114.38	114.92	115.50	116.19	116.29	128.4
C8	117.14	117.14	117.20	117.13	117.24	128.4
C10	131.75	131.64	131.58	131.41	131.35	139.5
C11	125.90	126.87	127.79	128.55	128.71	137.5
C12	13.31	13.11	12.96	12.65	12.71	19.80
C16	44.79	45.04	45.29	45.32	45.37	53.20
C20	128.28	129.29	130.24	131.16	131.31	139.5
C21	13.80	13.68	13.57	13.33	13.34	19.80
C25	14.45	14.53	14.60	14.59	14.60	21.10

Molecular electrostatic potential (MEP)

The molecular electrostatic potential (MEP) is used primarily for predicting sites and relative reactivity towards electrophilic and nucleophilic attacks, and in predicting the hydrogen bonding interactions [28,29]. The MEP of the *Z*-isomer calculated using B3LYP with 6-311++G(d,p) basis set is used to predict the reactive sites for electrophilic and nucleophilic attack. The negative (red) regions of the MEP are related to electrophilic reactivity, whereas the positive (blue) regions are related to nucleophilic reactivity (Fig. 6). As can be seen, negative regions are mainly localized over the oxygen atom whereas the maximum positive region is localized on the hydrogen atoms. The positive regions are associated with H4 and H18 with values around +0.0354 and +0.0314 a.u., respectively. Therefore, it is expected that the most preferred region for nucleophilic attack will be on H4 and H18. However, the most negative region is localized on atom O1 (with a value of −0.0589 a.u.) which will be the preferred site for electrophilic attack [30].

Electronic absorption spectra and frontier molecular orbitals (FMOs)

In order to understand the electronic transitions of the titled compound, the first twenty spin allowed singlet–singlet excitations were calculated using TD-DFT calculations in the gas phase. In these calculations, we have started from the gas phase optimized geometry of the *Z*-isomer using the same level of theory. Similar calculations were performed to get the excitation energies of *Z*-isomer in different solvents using the polarized continuum model (PCM). The results, which are shown in Table 6, represent the calculated λ_{max} values with their major contributions of molecular orbitals to the formation of bands for the *Z*-isomer. Of the twenty electronic transitions obtained from the current calculations, the only four transitions which have the highest oscillator strength (*f*) values are considered. These spectral bands are calculated at 285.1, 244.1, 217.2 and 205.9 nm in the gas phase. Experimentally, these transition bands are observed in water at 278, 250, 224 and 210 nm, respectively. In view of calculated absorption spectrum, the maximum absorption wavelength corresponds to the electronic transition from the HOMO to LUMO with 74% contribution. Fig. 7 shows the isodensity surface plots of

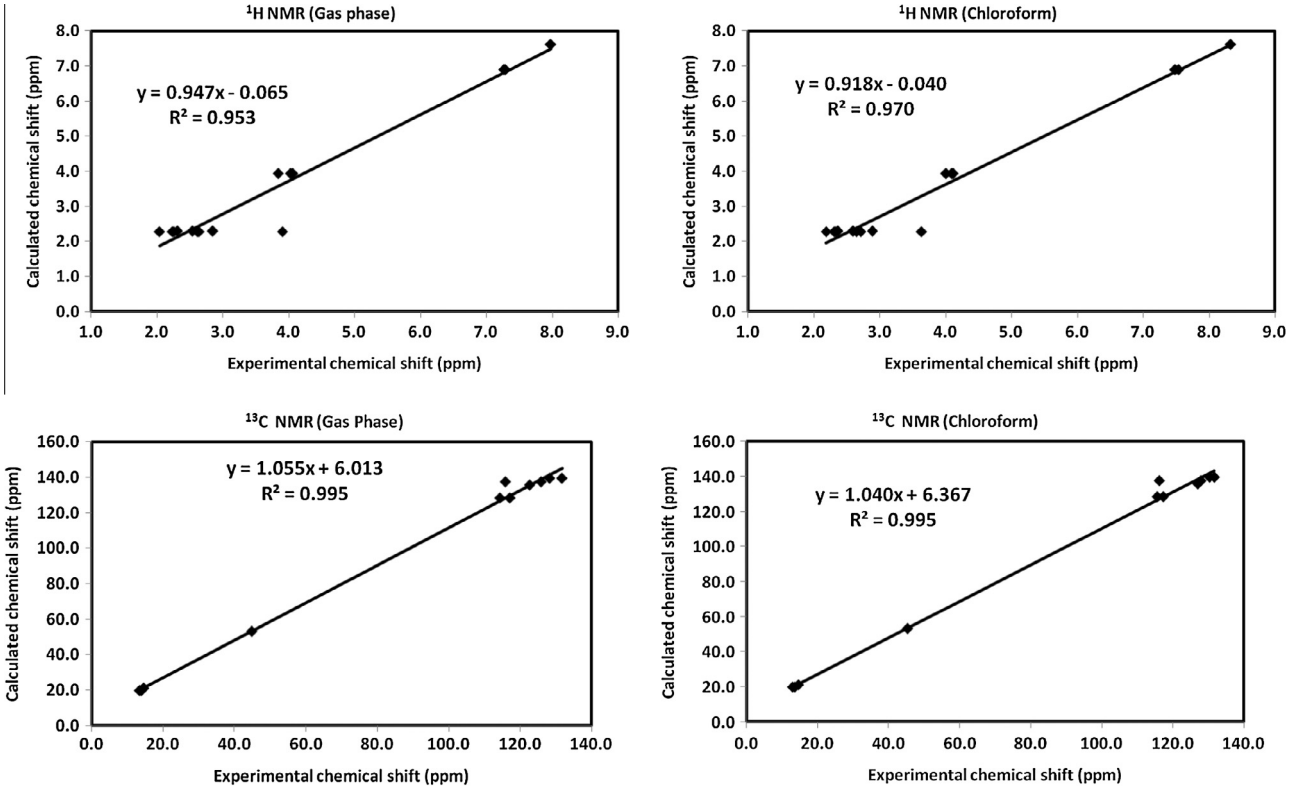

Fig. 9. Correlations between the experimental and calculated chemical shifts using the GIAO method.

Table 8
The second order perturbation energies $E^{(2)}$ (kJ/mol) of the most important charge transfer interactions (donor–acceptor) in the studied molecule using B3LYP method.

Donor NBO (i)	Acceptor NBO (j)	$E^{(2)}$[a] (kJ/mol)	$E(j)-E(i)$[b] (a.u.)	$F(i,j)$[c] (a.u.)
BD(2)C5—C10	BD*(2)N2—C3	64.10	0.2	0.05
	BD*(2)C6—C11	95.44	0.28	0.072
	BD*(2)C8—C20	70.29	0.28	0.062
BD(2)C6—C11	BD*(2)C5—C10	66.44	0.29	0.061
	BD*(2)C8—C20	92.51	0.29	0.071
BD(2)C8—C20	BD*(2)C5—C10	97.82	0.28	0.073
	BD*(2)C6—C11	72.47	0.28	0.062
LP(1)O1	BD*(1)N2—C3	23.81	1.29	0.077
LP(2)O1	BD*(1)N2—C3	30.46	0.77	0.067
	BD*(1)N2—C16	50.04	0.53	0.071
LP(3)O1	BD*(2)N2—C3	269.99	0.2	0.103
LP(1)O1	BD*(1)C12—H15	2.97	1.26	0.027

[a] $E^{(2)}$ means energy of hyperconjucative interactions.
[b] Energy difference between donor and acceptor i and j NBO orbitals.
[c] $F(i,j)$ is the Fock matrix element between i and j NBO orbitals.

molecular orbitals (MOs) contributed in this electronic transition. It can be seen from this figure that the electron densities of these MOs are mainly localized on the π-system of the *Z*-nitrone. Therefore, the band calculated at 285.1 nm is attributed mainly to a HOMO–LUMO transition that is predicted as $\pi \rightarrow \pi^*$ transition. The calculated electronic spectra of the *Z*-nitrone in different solvents compared to the gas phase are shown in Fig. 8. It can be seen that, the calculated absorption band at 285.1 nm in the gas phase showed only little spectral shift in all the studied solvents. In contrast, the rest of the spectral bands underwent either hypsochromic shift or hyperchromic effect in presence of solvent due to the solute–solvent interactions. The spectral shifts and the increase of absorption intensity are higher in polar solvents such as DMSO and water compared to nonpolar solvents such as cyclohexane.

Nonlinear optical effects

Nonlinear optical (NLO) materials have a great impact on information technology and industrial applications. The understanding of the relationships between the NLO activity and the electronic properties of any given compound has great importance for the development of new and more sophisticated materials with great NLO properties [31]. The polarizability (α) and the ability of electronic transition are important factors that affect the NLO activity of a compound. For comparative purposes, urea was used as reference for the NLO activity of the studied compound [32]. Our compound has higher polarizability (α = 152.72 Bohr^3) compared to urea (34.06 Bohr^3). It has also about five times higher NLO than urea. In addition, the HOMO–LUMO energy gap (ΔE) indicates the ease of the electronic transition and hence the ability of molecule to absorb light in visible region. The ΔE value of the studied compound is calculated to be 4.5713 eV which is lower than that for urea (6.7063 eV). Based on these theoretical data, the studied compound could be used as NLO material even better than urea.

NMR spectra

The isotropic magnetic shielding (IMS) values calculated using the GIAO approach at the 6-311++G(d,p) level are used to predict the ^{13}C and ^{1}H chemical shifts (δ_{calc}) for the *Z*-isomer. The results are correlated to the experimental NMR data (δ_{exp}) in $CDCl_3$ solvent. The solvent polarity effect is taken into account by the PCM model using different solvent models. The experimental and theoretical values for ^{1}H and ^{13}C NMR chemical shift values are given in Table 7. The correlation between the experimental and calculated chemical shifts is shown in Fig. 9. The results show that the correlation is better for carbon-13 than that for proton since protons are more affected by the solute intermolecular (solute–solvent) interaction than the carbons [33]. Also, the calculated chemical shifts in the appropriate solvent for predicting the ^{1}H NMR shifts is more efficient than that in gas phase.

Natural bond orbital analysis

The occupancy of electrons and p-character in significant NBO natural atomic hybrid orbitals for the studied compound is given in Table S7 (Supplementary Information). It is noted that, the hydrogen atoms have almost 0% of p-character for all C—H bonds. In contrast, 100% p-character was observed in atoms that have π-bonding of C—C and C—N bonds. Similarly, almost 100% p-character was observed in second and third lone pairs of O-atom.

It is well known that the ideal sp^2 hybrid orbital has 66.67% p-character. The BD(1)C5—C10 orbital with 1.9681 electrons has 50.92% C5 character (64.71%p) and 49.08% C10 character (66.48%p). Also, the BD(1)C6—C11 orbital with 1.9719 electrons has 49.67% C6 character (64.38%p) and 50.33% C11 character (64.91%p). The BD(1)N2—C3 orbital with 1.9911 electrons has 63.27% N2 character (59.49%p) and 36.73% C3 character (69.88%p). The low% p-character in these hybrids is due to the resonance effect with the phenyl group and the C=N bond. The two C-atoms forming the C—C hybrids have almost the same %electron density (%ED). Similarly, the BD(1)O1—N2 orbital with 1.9934 electrons has 49.34% O1 character (78.14%p) and 50.66% N2 character (71.41%p). As expected from the electronegativity values of C, N, and O atoms, the valence hybrids analyses of NBO orbitals showed that all the C—N and N—O bond orbitals are polarized towards the nitrogen and oxygen respectively. The overall polarity of the studied compound was found to be 3.416 D.

Second-order perturbation theory

NBO method provides significant information about interactions in both filled and virtual orbital spaces which could enhance the analysis of intra- and inter-molecular interactions. The stabilization energy $E^{(2)}$ associated with delocalization is estimated using the second-order perturbation theory [34]. The larger the $E^{(2)}$ value, the more intensive is the interaction between electron donors and electron acceptors [35]. Table 8 lists the calculated second order interaction energies ($E^{(2)}$) between the donor–acceptor orbitals in the studied molecule.

The most important interaction energy in this molecule, is the electron donating from LP(3)O1 orbital to the antibonding π*(2)-N2—C3 orbital which results in stabilization energy of 269.99 kJ/

Table 9
The calculated vibrational frequencies and intensities of the *Z*-isomer in gas phase and in solvents of different polarities using B3LYP/6-311++G(d,p) method.

No.	Gas		Cyclohexane		Chloroform		DMSO		Water		Exp	S.F	Assignment
	υ	A	Y	A	υ	A	υ	A	Y	A			
1	3210	15.3	3200	13.4	3185	9.4	3171	1.8	3171	2.1	3054	0.9513	$97\upsilon_{CH}$
2	3170	18.6	3169	8.0	3168	10.2	3153	3.0	3153	3.0	3040	0.9590	$91\upsilon_{CH}$
3	*3169*	7.5	3159	3.4	3156	3.1	3150	22.6	3139	26.1			$89\upsilon_{CH}$
4	3166	27.0	3157	15.5	3141	11.9	3126	11.4	3123	15.9			$94\upsilon_{CH}$
5	*3161*	4.3	3154	23.7	3139	20.0	3125	28.3	3123	35.9			$95\upsilon_{CH}$
6	*3121*	18.7	3121	20.5	3120	19.9	3119	11.2	3119	2.8			$96\upsilon_{CH}$
7	*3120*	14.3	3119	14.4	3119	12.5	3118	2.7	3118	3.1			$87\upsilon_{CH}$
8	*3119*	16.1	3118	18.8	3117	21.5	3116	23.0	3116	16.3			$90\upsilon_{CH}$
9	*3089*	13.4	3088	14.2	3088	14.1	3087	4.9	3087	8.8	2971	0.9617	$90\upsilon_{CH}$
10	*3089*	18.6	3088	19.5	3087	20.5	3087	30.6	3087	26.6			$94\upsilon_{CH}$
11	*3081*	16.7	3082	16.8	3081	16.8	3081	16.7	3081	16.5	2947	0.9564	$94\upsilon_{CH}$
12	3071	28.2	3070	24.5	3068	20.9	3066	17.1	3066	17.2			$100\upsilon_{CH}$
13	3032	25.8	3031	27.8	3031	29.5	3030	29.0	3030	28.6	2916	0.9617	$85\upsilon_{CH}$
14	3032	40.6	3030	40.1	3029	36.9	3028	25.6	3028	23.0			$84\upsilon_{CH}$
15	3027	37.1	3028	38.7	3027	38.0	3028	45.0	3028	46.4			$98\upsilon_{CH}$
16	1654	45.6	1653	58.6	1651	67.7	1653	64.3	1653	64.1	1656	1.0012	$80\upsilon_{CC}$
17	1639	38.2	1641	45.9	1643	58.1	1646	81.1	1645	82.9	1639	1.0003	$54\upsilon_{CN}$
18	1603	21.3	1602	25.1	1601	28.0	1601	28.7	1600	28.4	1610	1.0043	$54\upsilon_{CC}$
19	1519	8.5	1518	9.9	1517	10.5	1517	13.7	1516	14.3	1510	0.9939	$25\delta_{HCH}$
20	1511	22.9	1508	32.3	1506	36.1	1504	36.7	1504	36.2			$55\delta_{HCH}$
21	1510	25.4	1507	24.5	1503	28.2	1499	26.1	1498	27.4			$21\delta_{HCH}$
22	1497	3.3	1494	4.4	1491	6.0	1489	8.5	1488	8.7	1451	0.9694	$52\delta_{HCH}$
23	1492	13.3	1489	15.0	1486	16.0	1484	14.2	1483	13.1			$60\delta_{HCH} + 11\delta_{CCC}$
24	1492	8.4	1488	8.5	1485	8.6	1484	10.3	1483	10.9			$77\delta_{HCH}$
25	1482	7.3	1480	5.9	1478	6.5	1478	6.3	1477	6.4			$71\delta_{HCH}$
26	1474	35.7	1471	32.1	1469	33.0	1467	26.8	1466	25.8			$31\delta_{HCH}$
27	1472	20.1	1470	26.3	1468	26.5	1466	25.2	1465	27.5			$63\delta_{HCH} + 13\tau_{HCNC}$
28	1458	38.7	1453	58.3	1449	69.9	1444	63.4	1443	64.4			$11\upsilon_{NO} + 17\delta_{HCC} + 14\delta_{HCH}$
29	1443	1.8	1442	2.5	1441	3.3	1439	2.7	1439	2.2			$14\upsilon_{CC} + 14\delta_{HCC}$
30	1431	10.8	1431	20.3	1430	35.3	1428	67.2	1428	65.4			$12\delta_{HCC} + 56\delta_{HCH}$
31	1421	2.9	1420	4.7	1418	7.2	1417	11.1	1417	10.7	1412	0.9935	$63\delta_{HCH}$
32	1418	2.0	1416	2.0	1415	2.5	1413	1.7	1413	1.8			$61\delta_{HCH}$
33	1417	7.4	1415	7.0	1413	6.1	1411	9.1	1411	7.5	1371	0.9676	$73\delta_{HCH}$
34	1340	5.2	1338	7.6	1335	10.1	1330	10.8	1330	11.9			$47\upsilon_{CC}$
35	1311	1.3	1311	1.4	1311	1.4	1313	1.7	1312	1.7			$48\upsilon_{CC} + 23\delta_{CCC}$
36	1281	0.6	1281	0.7	1281	0.9	1281	1.2	1280	1.4			$11\upsilon_{CC} + 45\delta_{HCC}$
37	1248	0.6	1248	1.1	1248	1.9	1248	1.9	1247	2.7			$24\upsilon_{CC} + 13\delta_{CCC} + 31\delta_{HCC}$
38	1216	96.4	1210	136.7	1203	183.7	1195	219.2	1194	223.3	1181	0.9709	$42\upsilon_{NO} + 17\upsilon_{CN} + 18\delta_{HCC}$
39	1179	2.1	1178	5.2	1177	12.4	1176	30.4	1175	38.4	1153	0.9781	$12\upsilon_{CC} + 34\delta_{HCC}$
40	1140	1.0	1140	1.1	1140	1.3	1141	1.3	1141	1.4	1126	0.9875	$29\delta_{HCH} + 53\tau_{HCNC}$
41	1101	0.5	1103	0.8	1105	1.2	1106	1.8	1107	2.1	1095	0.9943	$10\upsilon_{CN} + 14\delta_{HCH} + 56\tau_{HCNC}$
42	1067	4.0	1066	5.1	1065	6.5	1064	6.6	1064	6.7			$11\delta_{HCH} + 34\tau_{HCCC}$
43	1061	0.4	1060	1.2	1059	2.1	1059	2.8	1059	3.1			$52\tau_{HCCC}$
44	1060	12.3	1059	15.1	1058	18.5	1058	19.7	1057	20.0			$15\delta_{HCH} + 47\tau_{HCCC}$
45	1056	0.9	1056	1.7	1055	3.6	1055	13.4	1055	14.0	1041	0.9857	$47\tau_{HCCC}$
46	1035	1.6	1034	1.8	1034	1.9	1034	1.8	1034	1.8			$11\delta_{HCH} + 44\tau_{HCCC}$
47	1033	2.1	1032	3.6	1032	5.2	1031	6.8	1031	7.3			$10\upsilon_{CC} + 48\tau_{HCCC}$
48	983	10.3	981	19.1	978	33.8	974	59.4	973	59.8	956	0.9727	$16\upsilon_{NO} + 22\upsilon_{CN}$
49	977	0.2	975	0.2	973	0.2	970	0.7	970	5.3			$50\upsilon_{CC}$
50	942	2.9	942	4.1	941	5.8	941	9.4	940	11.1	930	0.9872	$30\upsilon_{CC} + 10\upsilon_{CN} + 14\delta_{CCC}$
51	896	0.1	897	0.1	898	0.1	899	0.1	899	0.1			91τHCCC
52	868	22.6	868	29.6	869	39.8	870	53.9	870	55.5	858	0.9882	$68\tau_{HCCC} + 10\tau_{CCCC(OUT)}$
53	844	0.6	845	0.8	846	1.3	847	2.7	846	3.7	820	0.9714	$11\upsilon_{CC} + 15\upsilon_{CN}$
54	788	16.6	797	19.7	808	23.4	816	27.6	820	27.0			$68\tau_{HCCC} + 11\tau_{CCCN}$
55	728	1.3	728	2.0	728	3.1	726	4.6	726	5.8	720	0.9883	$11\delta_{CCC} + 39\tau_{CCCC}$
56	622	9.9	621	10.5	619	10.3	618	9.6	618	8.9	617	0.9923	$42\tau_{OCCN(OUT)}$
57	616	2.2	616	3.0	615	4.0	615	5.5	614	5.2			$14\upsilon_{CN} + 11\delta_{CCN} + 21\delta_{CCC}$
58	575	0.2	574	0.2	574	0.3	573	0.4	573	0.4	547	0.9517	52υCC
59	558	2.9	558	3.4	558	3.7	559	4.3	558	4.2			$10\tau_{OCCN(OUT)} + 26\tau_{CCCC(OUT)}$
60	543	1.3	542	1.4	540	1.6	538	2.1	538	2.2	537	0.9884	$10\upsilon_{CC} + 29\delta_{CCC} + 12\tau_{OCCN(OUT)}$
61	528	0.7	528	0.9	529	1.2	529	1.5	529	1.6			$57\tau_{CCCC(OUT)}$
62	510	7.2	509	9.0	508	8.3	506	9.4	506	11.5	508	0.9959	$66\delta_{CCC}$
63	507	4.0	507	5.4	506	9.4	505	11.4	505	9.5	3054	0.9513	$14\delta_{CCC} + 23\delta_{ONC}$
64	377	1.5	376	2.2	376	3.3	374	4.9	374	4.7			$12\tau_{CNCC} + 21\tau_{CCCC(OUT)}$
65	354	7.7	354	11.1	353	14.7	352	17.1	352	18.1			$13\delta_{CCC} + 34\delta_{CNC}$
66	328	0.5	329	0.4	329	0.3	330	0.1	330	0.1			$58\delta_{CCC}$
67	293	1.8	290	1.9	286	1.7	282	1.6	282	1.6			$70\delta_{CCC}$
68	280	0.3	278	0.4	276	0.4	273	0.4	273	0.4			$26\delta_{CCC} + 12\delta_{CNC}$
69	238	1.2	237	1.6	237	1.9	236	1.6	236	1.7			$51\tau_{CCCC} + {}_{18}\tau_{CCCC(OUT)}$
70	199	6.7	197	7.3	196	3.9	196	5.2	197	5.3			$29\tau_{CCCC} + 75\tau_{CCCC(OUT)}$
71	196	1.7	195	5.4	193	14.6	186	19.5	186	21.1			$54\tau_{HCNC}$
72	178	0.4	177	0.5	177	0.7	177	2.0	176	1.7			$43\tau_{CCCC}$
73	163	1.4	158	1.6	153	1.8	142	3.8	142	2.7			$57\tau_{CCCC}$

Table 9 (*continued*)

No.	Gas		Cyclohexane		Chloroform		DMSO		Water		Exp	S.F	Assignment
	υ	A	Y	A	υ	A	υ	A	Y	A			
74	142	2.6	141	3.5	137	4.5	139	3.8	137	4.4			$55\tau_{CCCC}$
75	104	0.9	103	1.6	102	2.5	100	3.9	100	4.8			$58\tau_{CCCN}$
76	89	8.5	88	10.5	87	13.1	83	16.9	85	16.7			$12\delta_{CCC} + 10\tau_{CCCC} + 43\tau_{CNCC}$
77	64	1.8	64	2.1	65	2.4	65	3.1	65	3.1			$92\tau_{CCCC}$
78	22	0.2	15	0.2	17	0.3	46	0.3	46	0.3			$66\tau_{ONCC}$

mol. The π(C—C) → π*(C—C) interactions are responsible for conjugation of respective π-bonds within ring leading to a maximum stabilization energy of 97.82 kJ/mol. The π(C—C) → π*(C—N) interactions that stabilizes the molecule by up to 64.10 kJ/mol. The charge transfer interactions are formed by the orbital overlap between bonding (π) and antibonding (π*) orbitals, which results in intramolecular charge transfer (ICT) leading to extra stabilization of the system. NBO analysis clearly manifests the evidence for the weak intramolecular charge transfer from LP(1)O1 to π*(1)C12—H15 antibonding orbital. This confirms the presence of non-conventional interaction (C12—H15---O1) that provides up to 2.97 kJ/mol stabilization for the molecule.

Analysis of the vibrational spectra

The vibrational spectra of the most stable isomer (*Z*) of the studied compound has been calculated using the B3LYP/6-311++G(d,p) method. The FTIR spectrum of the studied compound is shown in Fig. S2 (Supplementary Information). The calculated vibrational frequencies and intensities together with the scaling factors (S.F) using the B3LYP/6-311++G(d,p) method are given in Table 9. The assignment of these modes based on the total energy distribution (TED) is given in the same table. The studied nitrone consists of 28 atoms. So, it has 78 normal vibrational modes. Herein we will provide description of the fundamental IR characteristics of the studied compound.

C—H vibrations

The studied nitrone has three C(sp^2)—H bonds. Therefore, it undergoes three C—H stretching vibrations that are observed in the range of 3040–3054 cm^{-1}. The B3LYP method predicted the υ(C—H) mode of the HC═N stretching vibration at 3210 cm^{-1}. The aromatic symmetric and asymmetrical stretching vibrations are predicted at 3170 and 3166 cm^{-1}, respectively. In aromatic compounds, the C—H in-plane bending vibrations are observed in the region 1300–850 cm^{-1} and are usually weak [36]. The C—H out of plane bending modes [37–39] are usually of medium intensity that arise in the region of 950–600 cm^{-1} [36]. The present DFT calculations predicted the in-plane C—H bending in the regions 1458–1431 and 1281–1179 cm^{-1}, whereas the out of plane C—H bending are predicted in the regions 1067–1033 and 896–788 cm^{-1}.

Methyl group vibrations

According to Pulay et al. [40], the methyl (CH_3) group has five types of vibrational frequencies namely: symmetric stretch, asymmetric stretch, symmetric deformation, asymmetric deformation and rocking. The studied molecule has four methyl groups; three of them are directly attached to the phenyl ring and the fourth is attached to the nitrogen of the N═C bond. The three methyl (CH_3) groups attached to the phenyl ring have nine C—H stretching vibrations: six asymmetric υ(C—H) modes occur in the region (3121–3081 cm^{-1}) and three symmetric υ(C—H) modes occur in the region (3032–3027 cm^{-1}). The asymmetric C—H stretches of the CH_3—N═C are predicted at 3169 and 3161 cm^{-1} whereas the symmetric one is predicted at 3071 cm^{-1}.

The asymmetric and symmetric bending vibrations of methyl groups normally appear in the region 1470–1440 cm^{-1} and 1390–1370 cm^{-1}, respectively [41–44]. The calculations predicted them in the ranges; 1519–1458 cm^{-1} and 1431–1417 cm^{-1}, respectively.

The rocking vibrations of the CH_3 group appear as mixed vibrations in the region 1170–1100 cm^{-1} [41–44]. Our calculations revealed that CH_3 rocking modes, which are coupled with other vibration modes, were predicted at lower frequency region (1140–1035 cm^{-1}; except modes 43 and 45).

C—C and C—N vibrations

The ring C═C stretching vibrations usually occur in the region of 1625–1430 cm^{-1} [45]. In the present work, the calculated value for benzene ring C═C vibrations were found at 1654 cm^{-1}, 1603 cm^{-1} and 1443 cm^{-1}. The C═N stretching vibration is calculated to be 1639 cm^{-1} which is exactly the same as that observed in experimental FT-IR spectrum. These results correlate well with the reported values in the literature [46,47].

Effect of solvent on the vibrational spectra

The effect of different solvents on the IR vibrational spectra (vibrational frequencies and vibrational intensities) is shown in Table 9 and Fig. S3 (Supplementary Information). As can be seen, the most significant variations in the vibrational frequencies and vibrational intensities occur only for the C═N and the C—H stretching modes. Most of these stretching modes undergo stronger bathochromic shifts in the presence of polar solvents such as water and DMSO compared to non-polar solvent (cyclohexane). Generally, an increase in the vibrational intensities in all solvent was noted compared to the gas phase. The increase of IR intensities was found to be dependent on the solvent polarity. The general trend for the IR intensity was found to be: water > DMSO > chloroform > cyclohexane > gas phase (Fig. S3, Supplementary Information). Most of the other modes are almost unaffected by the solvent.

Conclusions

In this work, the synthesis and characterization of the *N*-methyl-*C*-2,4,6-trimethylphenylnitrone **1** is reported. This compound has been characterized using different spectroscopic tools. DFT calculations showed that the *Z*-isomer is the most stable in the gas phase. The stability and population of the *E*-isomer is higher in polar solvents than in nonpolar. The molecular structure of the most stable isomer (*Z*) has been calculated and compared with the X-ray structure data. The effect of solvent on the structural parameters of the studied compounds was reported. Complete assignment of the vibrational modes has been performed on the basis of total energy distribution (TED) analysis. The TD-DFT showed that most of the spectral bands undergo either hypsochromic shift or hyperchromic effect in the presence of the solvent compared to the gas phase. The longest wavelength band at

285.1 nm (f_{osc} = 0.3543) in the gas phase showed a little spectral shift in all the studied solvents. The studied nitrone has been predicted to have better nonlinear optical properties (NLO) than urea. The second order perturbation theory has been used to predict the different intramolecular charge transfer (ICT) interactions within the studied molecules.

Acknowledgment

This work has been partially supported by the King Abdulaziz University (Rabigh Branch, Saudi Arabia).

Appendix A. Supplementary material

Supplementary data associated with this article can be found, in the online version, at http://dx.doi.org/10.1016/j.saa.2014.10.096.

References

[1] L. Smith, Chem. Rev. 23 (1938) 193.
[2] J. Hamer, A. Macaluso, Chem. Rev. 64 (1964) 473.
[3] A. Padwa, W.H. Pearson, Synthetic Application of 1,3,-Dipolar Cycloaddition Chemistry Toward Heterocycles and Natural Products, Wiley, New Jersey, 2003.
[4] J. Lasri, M.A. Januário Charmier, M. Haukka, A.J.L. Pombeiro, J. Org. Chem. 72 (2007) 750.
[5] R.A. Floyd, R.D. Kopke, C.-H. Choi, S.B. Foster, S. Doblas, R.A. Towner, Free Radic. Biol. Med. 45 (2008) 1361.
[6] A. Herbrectsmier, F.-M. Schnepel, O. Glemser, J. Mol. Struct. 50 (1978) 43.
[7] N.S. Ferris, W.H. Woodruff, D.B. Rorabacher, T.E. Jones, L.A. Ochrymocoycz, J. Am. Chem. Soc. 100 (1978) 5939.
[8] R.A. Floyd, H.K. Chandru, T. He, R. Towner, Anticancer Agents Med. Chem. 11 (2011) 373.
[9] C.H. Choi, K. Chen, A. Vasquez-Weldon, R.L. Jackson, R.A. Floyd, R.D. Kopke, Free Radic. Biol. Med. 44 (2008) 1772.
[10] I.A. Sekine, A. Masuko, K. Senoo, Corros. Sci. 43 (1987) 553.
[11] M.A. Quarishi, D. Jamal, Corros. Sci. 56 (2000) 156.
[12] E. Heitz, Advances in Corrosion Science and Technology, vol. 4, Plenum Press, New York, NY, 1974.
[13] M.Z.A. Rafiquee, S. Khan, N. Saxena, M.A. Quaraishi, Port. Spectrochim. Acta 25 (2007) 419.
[14] Y. Inouye, J. Hara, H. Kakisawa, Chem. Lett. (1980) 1407.
[15] N.R. Sheela, S. Sampathkrishnan, M. Thirumalai Kumar, S. Muthu, Spectrochim. Acta A 112 (2013) 62.
[16] N.R. Sheela, S. Sampathkrishnan, M. Thirumalai Kumar, S. Muthu, Spectrochim. Acta A 109 (2013) 272.
[17] Agilent, CrysAlisPro, Agilent Technologies inc., Yarnton, Oxfordshire, England, 2012.
[18] G.M. Sheldrick, Acta Crystallogr. Sec. A 64 (2008) 112.
[19] O.V. Dolomanov, L.J. Bourhis, R.J. Gildea, J.A.K. Howard, H. Puschmann, J. Appl. Cryst. 42 (2009) 339.
[20] E.F. Pettersen, T.D. Goddard, C.C. Huang, G.S. Couch, D.M. Greenblatt, E.C. Meng, T.E. Ferrin, J. Comput. Chem. 25 (2004) 1605.
[21] M.J. Frisch, et al., Gaussian-03, Revision C.01, Gaussian Inc, Wallingford, CT, 2004.
[22] R. Dennington II, T. Keith, J. Millam, GaussView, Version 4.1, Semichem Inc., Shawnee Mission, KS, 2007.
[23] A.D. Becke, Phys. Rev. A 38 (1988) 3098.
[24] W. Wang, W.J. Mortier, J. Am. Chem. Soc. 108 (1986) 5708.
[25] M.H. Jamroz, Vibrational Energy Distribution Analysis VEDA 4, Warsaw, 2004.
[26] E.D. Glendening, A.E. Reed, J.E. Carpenter, F. Weinhold, NBO Version 3.1, CI, University of Wisconsin, Madison, 1998.
[27] R. Sustmann, W. Sicking, R. Huisgan, J. Am. Chem. Soc. 117 (1995) 9679.
[28] J.S. Murray, K. Sen, Molecular Electrostatic Potentials, Concepts and Applications, Elsevier, Amsterdam, 1996.
[29] E. Scrocco, J. Tomasi, Adv. Quant. Chem. 11 (1978) 115.
[30] B. Galabov, D. Cheshmedzhieva, S. Ilieva, B. Hadjieva, J. Phys. Chem. A 108 (2004) 11457.
[31] D. Arivuoli, PRAMANA – J. Phys. 57 (2001) 871.
[32] C. Sridevi, N.P. Selvam, G. Shanthi, G. Velraj, J. Mol. Struct. 1030 (2012) 46.
[33] B. Osmiałowski, K. Kolehmainen, R. Gawinecki, Magn. Res. Chem. 39 (2001) 334.
[34] J. Chocholousova, V. Vladimir Spirko, P. Hobza, J. Phys. Chem. Chem. Phys. 6 (2004) 37.
[35] S. Sebastian, N. Sundaraganesan, Spectrochim. Acta Part A 75 (2010) 941.
[36] V. Arjunan, P. Ravindran, T. Rani, S. Mohan, J. Mol. Struct. 988 (2011) 91.
[37] V. Arjunan, S. Mohan, S. Subramanian, B. Thimme Gowda, Spectrochim. Acta 60A (2004) 1141.
[38] V. Arjunan, N. Puviarasan, S. Mohan, Spectrochim. Acta 64A (2006) 233.
[39] A. Altun, K. Golcuk, M. Kumru, J. Mol. Struct.: Theochem. 637 (2003) 155.
[40] P. Pulay, G. Fogarasi, F. Pang, J.E. Boggs, J. Am. Chem. Soc. 101 (1979) 2550.
[41] B. Smith, Infrared Spectral Interpretation, A Systematic Approach, CRC Press, Washington, DC, 1999.
[42] N.B. Colthup, L.H. Daly, S.E. Wiberley, Introduction to Infrared and Raman Spectroscopy, Academic Press, New York, 1990.
[43] F.R. Dollish, W.G. Fateley, F.F. Bentley, Characteristic Raman Frequencies of Organic Compounds, John Wiley & Sons, New York, 1997.
[44] L.J. Bellamy, The Infra-red Spectra of Complex Molecules, John Wiley and Sons Inc., New York, 1975.
[45] D.L. Pavia, G.M. Lampman, G.S. Kriz, Introduction to Spectroscopy, Harcourt College Publishers, 2001.
[46] A.D. Becke, J. Chem. Phys. 98 (1993) 5648.
[47] C.T. Lee, W.T. Yang, R.G.B. Parr, Phys. Rev. 37 (1988) 785.